

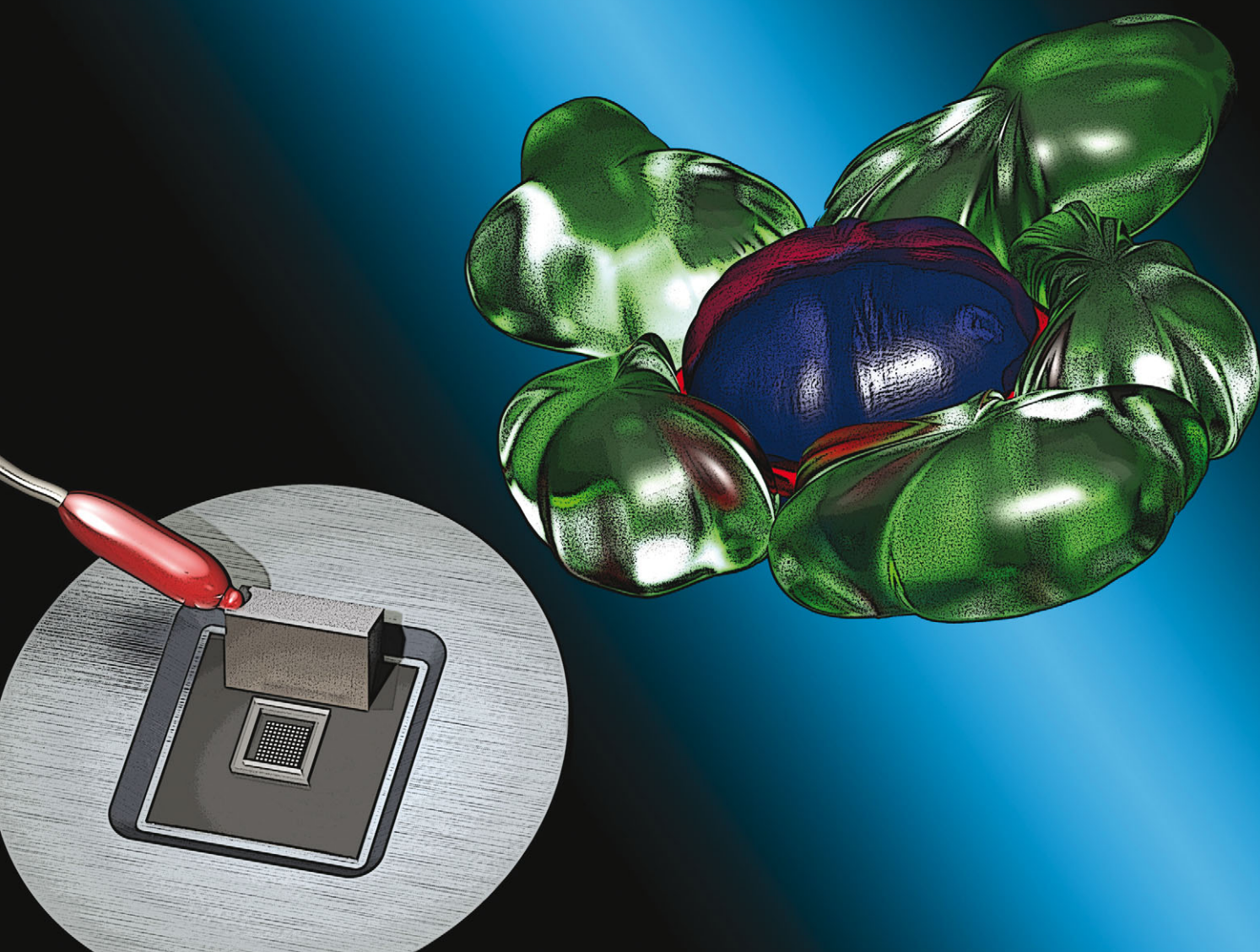
Indexed in  
**MEDLINE!**

# Integrative Biology

Interdisciplinary approaches for molecular and cellular life sciences

[www.rsc.org/ibiology](http://www.rsc.org/ibiology)

Volume 5 | Number 4 | April 2013 | Pages 643–740



ISSN 1757-9694

RSC Publishing

**TECHNICAL INNOVATION**

Athanasia Christakou, Björn Önfelt *et al.*

Live cell imaging in a micro-array of acoustic traps facilitates quantification of natural killer cell heterogeneity



1757-9694(2013)5:4;1-P

## Live cell imaging in a micro-array of acoustic traps facilitates quantification of natural killer cell heterogeneity†

Cite this: *Integr. Biol.*, 2013, 5, 712

Athanasia E. Christakou,<sup>a</sup> Mathias Ohlin,<sup>a</sup> Bruno Vanherberghen,<sup>a</sup> Mohammad Ali Khorshidi,<sup>a</sup> Nadir Kadri,<sup>b</sup> Thomas Frisk,<sup>a</sup> Martin Wiklund<sup>a</sup> and Björn Önfelt<sup>\*abc</sup>

Natural killer (NK) cells kill virus-infected or cancer cells through the release of cytotoxic granules into a tight intercellular contact. NK cell populations comprise individual cells with varying sensitivity to distinct input signals, leading to disparate responses. To resolve this NK cell heterogeneity, we have designed a novel assay based on ultrasound-assisted cell–cell aggregation in a multiwell chip allowing high-resolution time-lapse imaging of one hundred NK–target cell interactions in parallel. Studying human NK cells' ability to kill MHC class I deficient tumor cells, we show that approximately two thirds of the NK cells display cytotoxicity, with some NK cells being particularly active, killing up to six target cells during the assay. We also report that simultaneous interaction with several susceptible target cells increases the cytotoxic responsiveness of NK cells, which could be coupled to a previously unknown regulatory mechanism with implications for NK-mediated tumor elimination.

Received 18th October 2012,  
Accepted 3rd February 2013

DOI: 10.1039/c3ib20253d

[www.rsc.org/ibiology](http://www.rsc.org/ibiology)

### Insight, innovation, integration

Recent studies have indicated that natural killer (NK) cells' cytotoxic response against aberrant cells varies between individual NK cells. To understand how NK cells assist the immune system to fight disease new methods are needed by which the response of individual cells can be studied. We present a novel assay based on ultrasound-assisted cell–cell aggregation, allowing time-lapse imaging of multiple NK–target cell interactions in parallel. We quantify the fraction of cytotoxic NK cells, describe a subpopulation capable of killing several target cells and show that NK cytotoxicity increases with stimulation from several target cells. By inducing cell–cell contact, we effectively bypass the step of migration and can focus on studying immune synapse formation and NK cytotoxicity in a controlled manner.

## Introduction

NK cells are lymphocytes capable of recognizing virus-infected or tumor-transformed cells. The NK cell immune response includes secretion of cytokines and/or direct killing of aberrant cells through the release of cytotoxic granules into the tight intercellular contact, *i.e.* the immune synapse, formed between the NK and target cells. NK cell activity is regulated by the integration of inhibitory and activating signals at the immune synapse where NK cell receptors engage with cognate ligands

on the target cell. A central question is how NK cells are 'educated' to tune the threshold for activation so that each organism can be protected from infections and tumor transformations without development of NK cell autoimmunity.

Previous studies have shown that NK cell education is linked to the type and expression level of inhibitory MHC class I ligands expressed by the host.<sup>1</sup> Genetic variability leads to both great differences in MHC class I expression patterns as well as a large range of NK cell activation thresholds between individuals. This can, for example, be exploited to achieve anti-tumor effects in stem cell transplantations.<sup>2</sup> Experiments in mice have also shown that NK cell education leads to considerable heterogeneity in the activation threshold and response of individual NK cells.<sup>3–5</sup> This underlines the importance of developing new methods allowing the response of many individual cells to be studied.

Several microchip-based assays have been developed for single cell studies with imaging or screening read-outs;

<sup>a</sup> Department of Applied Physics, Albanova University Center, KTH - Royal Institute of Technology, SE-10691, Stockholm, Sweden. E-mail: [bjorn.onfelt@ki.se](mailto:bjorn.onfelt@ki.se); Tel: +46 8 55378793, +46 730 766146

<sup>b</sup> Department of Microbiology, Tumor and Cell Biology, Karolinska Institute, Nobels Väg 16, 17177, Stockholm, Sweden

<sup>c</sup> Science for Life Laboratory, Tomtebodavägen 23A, 17165 Stockholm, Sweden

† Electronic supplementary information (ESI) available. See DOI: 10.1039/c3ib20253d

however, few are optimized for dynamic, real-time studies of cell–cell interactions (see for example ref. 6–10). A common approach has been to confine cells in miniature wells and wait for them to interact.<sup>10–14</sup> The time required for this is a function of the migration properties, size of the cells and size of the wells.<sup>11</sup> Hence, the actual timing of cell–cell contact is not well controlled (*i.e.* synchronized) in these devices. However, for high-throughput screening of dynamic interactions, such as NK–target cell interactions, the timing of cell–cell contact is important. Here, we use a novel method where ultrasonic standing waves are used to aggregate and position cells in the center of one hundred,  $300 \times 300 \mu\text{m}^2$  microwells in a controlled manner.<sup>8,15</sup> We show that it is possible to induce synchronized contact between NK and target cells with forces comparable to biological forces, *e.g.* adhesion to other cells, and that vital NK cell functions are preserved under the exposure to ultrasound. Finally, we use the device in a killing assay, where the lytic activity of individual NK cells can be detected, to show that there is heterogeneity in individual NK cells' capacity to eliminate MHC class I deficient tumor target cells.

## Methods

### Device design, fabrication and operation

Microfabrication has been described previously.<sup>16</sup> Briefly, 4" silicon wafers, 300  $\mu\text{m}$  thick, were cleaned and wet oxidized before a positive photo resist AZ 9260 (MicroChemicals GmbH, Ulm, Germany) was spun on to them. The mask was aligned, exposed (Mask Aligner, MicroTec MA/BA6, SÜSS MicroTec Lithography GmbH, Garching, Germany) and baked before the oxide pattern was dry-etched (Precision 5000 Mark II, Applied Materials, Austin, Texas, USA). The silicon wells were then deep-etched by dry ion plasma (STS ICP, Surface Technology Systems, Newport, UK) and cleaned by oxygen plasma followed by a wet cleaning in a mixture of  $\text{H}_2\text{SO}_4$  and  $\text{H}_2\text{O}_2$  (3 : 1). The wafers were again wet oxidized at 1100 °C to increase the biocompatibility. Finally, a 175  $\mu\text{m}$  thick glass slide was bonded to the silicon wafer before dicing into microchips with a  $22 \times 22 \text{ mm}^2$  footprint. Here, the microchips had  $10 \times 10$  centrally positioned square wells covering an area of  $3.9 \times 3.9 \text{ mm}^2$  (each well with a  $300 \times 300 \mu\text{m}^2$  bottom area separated by 100  $\mu\text{m}$  walls). The gasket was created from a 1 mm thick slab of polydimethylsiloxane (PDMS) that was cut and plasma-bonded to the silicon surface creating a  $\sim 50 \mu\text{l}$  basin above the microwells. The silicon chip was glued into the metal holder using a thin cork layer between the chip and the holder to avoid energy loss during ultrasonic actuation. Finally, a wedge transducer was glued with a thin layer of tensile conductive adhesive gel (BBS Medical AB) onto the chip. Ultrasonic actuation was performed by cycling linear frequency sweeps (saw-tooth modulation) with a center frequency of 2.54 MHz, a bandwidth of 120 kHz, a modulation rate of 1 kHz and an actuation voltage between 0 and 10  $V_{\text{pp}}$ . In all experiments not examining the voltage dependence, the actuation voltage was 10  $V_{\text{pp}}$ . The ultrasonic actuation leads to a slight temperature increase,<sup>8</sup>

which was compensated for by setting the thermostat of the environmental chamber to  $33.5 \pm 0.5$  °C, leading to a stable temperature of 37 °C of the sample.

### Preparation and culture of peripheral blood NK cells

Polyclonal primary human NK cells were isolated from lymphocyte-enriched buffy coat residues derived from healthy donors. Briefly, peripheral blood mononuclear cells (PBMCs) were isolated from buffy coat by centrifugation on Ficoll-Paque Plus according to the manufacturer's instructions (GE Healthcare). NK cells isolation was performed by negative immunomagnetic bead isolation (EasySep<sup>®</sup> Human NK Cell Enrichment Kit, StemCell Technologies) according to the manufacturer's instructions. Primary NK cells were cultured in Iscove's modified Dulbecco's medium (IMDM, I3390, Sigma-Aldrich, St. Louis, MO, USA), supplemented with 10% autologous human serum, 2 mM L-glutamine (G7513 Sigma-Aldrich, St. Louis, MO, USA), 100  $\text{U ml}^{-1}$  penicillin–100  $\mu\text{g ml}^{-1}$  streptomycin (P4333; Sigma Aldrich, St. Louis MO, USA),  $1 \times$  non-essential amino acids (M7145, Sigma-Aldrich, St. Louis, MO, USA), 1 mM sodium pyruvate (S8636, Sigma-Aldrich, St. Louis, MO, USA) and 200  $\text{U ml}^{-1}$  human interleukin (IL)-2 (PeproTech, Rocky Hill, NJ, USA) for one week prior to the experiments. NK cells were  $\sim 99.5\%$   $\text{CD3}^- \text{CD56}^+$  and their killing capacity was confirmed by conventional cytotoxicity assay against 221 cells.<sup>17</sup>

### Cell lines

The human B lymphoblastoid cell line 721.221 (referred to as 221) was used both as a model for non-adherent cells and as a NK target. This cell line was selected since it lacks endogenous MHC class I expression and is susceptible to NK-mediated killing. For studies of the inhibitory NK cell synapse, 721.221 transfected to express green fluorescent protein (GFP)-tagged MHC/HLA-Cw6 was used (721.221/Cw6-GFP) in combination with the human NK cell line YTS transfected to express the inhibitory NK cell receptor KIR2DL1.<sup>18</sup> Human embryonic kidney cells 293T (HEK293T) were used as a model for adherent cells. All cell lines were cultured in RPMI-1640 (SH30027 Thermo Scientific, MA, USA) supplemented with 10% fetal bovine serum (SV30160; Thermo Scientific, MA, USA), and 100  $\text{U ml}^{-1}$  penicillin–100  $\mu\text{g ml}^{-1}$  streptomycin,  $1 \times$  non-essential amino acids, 1 mM sodium pyruvate and maintained at 37 °C, 5%  $\text{CO}_2$ .

### Cell labeling

The fluorescent viability dyes used were calcein green-AM and calcein red-orange-AM (Invitrogen, Carlsbad, CA, USA). Far red DDAO-SE (Invitrogen, Carlsbad, CA, USA) was used for long-term cell labeling. Cells were washed twice in RPMI-1640 and centrifuged for 10 min at  $400 \times g$  to a pellet. The staining solution, prepared by dissolving the dyes in warm (37 °C) RPMI-1640, was added directly to the cell pellet. Dye concentrations used for monitoring of NK cell mediated killing were 0.25  $\mu\text{M}$  for calcein green, 0.32  $\mu\text{M}$  for calcein red-orange and 1  $\mu\text{M}$  for DDAO. For the adherent and non-adherent cell trapping experiments 293T cells were stained with 0.5–1  $\mu\text{M}$  calcein green.

For the long-term tracking experiments of cell clusters, we used 0.5  $\mu\text{M}$  for both calcein green (for 221) and calcein red-orange (for NK cells) and 10  $\mu\text{M}$  for DDAO (for 221). For high resolution imaging of the immune synapse, YTS were stained with 6  $\mu\text{M}$  DDAO. For all stainings, cells were resuspended and incubated for 10 minutes (except YTS cells, which were incubated for 15 minutes). Stained cells were washed twice in RPMI-1640 and resuspended in culture medium before being used.

### Flow cytometry

For surface staining, isolated human peripheral blood NK cells were incubated in 50  $\mu\text{l}$  FACS buffer (PBS, 2% FCS) containing monoclonal antibodies to CD56 (0.5  $\mu\text{g ml}^{-1}$ , clone: B159) and CD3 (0.1  $\mu\text{g ml}^{-1}$ , clone: UCHT1) (BD Pharmingen, San Diego, CA) on ice for 20 min, washed in cold FACS buffer and resuspended in 200  $\mu\text{l}$  of FACS buffer before analysis with flow cytometry (LSRII, BD). Data were analyzed using FlowJo (Tree Star).

### Bulk cytotoxicity assay

NK cell bulk cytotoxicity was measured by conventional chromium release assay.<sup>17</sup> Target cells (221) were grown to mid-log phase, and  $0.5\text{--}1 \times 10^6$  cells were labeled in 100  $\mu\text{l}$  of culture medium with 30  $\mu\text{Ci}$   $^{51}\text{Cr}$  for 1 h at 37  $^{\circ}\text{C}$ . Cells were washed twice and resuspended in culture medium. NK cells were distributed on a V-bottom 96-well plate, and mixed with labeled target cells at different E:T ratios. The number of target cells was kept constant at 5000 cells per well with varying numbers of NK cells. After a 1 min centrifugation at  $300\times g$ , plates were incubated for 4 h at 37  $^{\circ}\text{C}$ . Supernatant was harvested and  $^{51}\text{Cr}$  release was measured in a gamma counter. Maximum release was determined by lysis of all target cells in the wells and spontaneous target cell death was assessed from wells incubated without NK cells. All samples were performed in triplicates.

### Microscopy

Images were acquired using an inverted laser scanning confocal microscope (LCSM, Zeiss LSM 5 Pascal) equipped with a motorized stage. Fluorescent microscopy imaging was performed using a dichroic beam-splitter HFT488/543/633 and different combinations of excitation wavelengths and emission filters depending on the staining probes: calcein green (Ex: 488 nm/Em: BP505-530); calcein red-orange (Ex: 543 nm/Em: BP560-615); DDAO (Ex: 633 nm/Em: LP650). Trapping of adherent and non-adherent cells under different voltage actuations was imaged using a  $2.5\times/0.075$  objective allowing imaging of all 100 wells in the same field of view. For cell cluster tracking and NK-mediated target cell killing experiments, a  $10\times/0.3$  objective was used. All wells could be imaged in a time-lapse manner using the moving stage to form a  $4 \times 4$  tile scan repeated every  $6.8 \pm 0.6$  minutes. For cell cluster tracking the time-lapse imaging lasted 17 hours, while the NK killing experiments were performed for 4 hours. Imaging with the  $10\times$  objective was performed with the confocal pinhole opened to maximize detection of fluorescent light. High-resolution imaging of the immune synapse was performed using bi-directional

LSCM, capturing 28  $1 \mu\text{m}$  Z slices (pinhole at airy 1) every 75 seconds for  $\sim 2$  hours using a  $100\times/1.3$  oil objective.

### Image analysis

Target cell death was scored by visual inspection of the target cell calcein and DDAO fluorescence in conjunction with looking for morphological features (*e.g.* cell blebbing) of target cell death in the bright-field image. The Volocity software package (Perkin Elmer) was used for 3D reconstruction of high-resolution confocal images of immune synapses. For automatic tracking of cell clusters aggregated in microwells, individual clusters were segmented from the background by intensity thresholding the fluorescence image and the center of each cluster calculated for each time point of the movie. From these trajectories the average distance from cluster centers and their corresponding well centers were measured at every time point of the experiment.

### Statistical analysis

Yates' chi-square test was used to evaluate the significance of increased frequency killing with the number of NK cells in each well. Fisher's exact test was used to evaluate if the variation in the frequency of killing found for single NK cells with varying numbers of target cells was significant.

## Results

### Multiwell ultrasonic device

The device consists of a 100-well silicon-glass microchip, a gasket that creates a basin for cell suspension, a custom-made metal holder to fit the microscope stage, and an ultrasound transducer (Fig. 1). This method allows simultaneous, parallelized trapping of cells in the center of multiple wells using ultrasonic standing waves without affecting cell viability.<sup>8</sup>

### Ultrasound aggregates non-adherent cells at forces balanced with biological processes

We wanted to compare the ultrasonic forces generated in the device with forces present in biological systems, *e.g.* adhesion to substrates or other cells. To this end, adherent HEK 293T

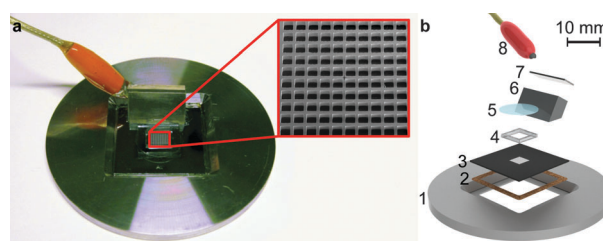


**Fig. 1** The ultrasonic device and its components. (a) Photograph of the multi-well set-up. The zoomed region shows a scanning electron microscopy image of the  $10 \times 10$  microwells. (b) The device consists of the multi-well silicon-glass microchip (3) glued to a stainless steel holder (1) through a thin cork frame (2) in order to avoid energy loss, a PDMS frame plasma bonded around the wells (4), and a cover glass (5) to avoid evaporation of the medium. The transducer operates around 2.5 MHz and consists of a titanium wedge (6), a piezoelectric thin ceramic plate (7) and a connecting cable (8).

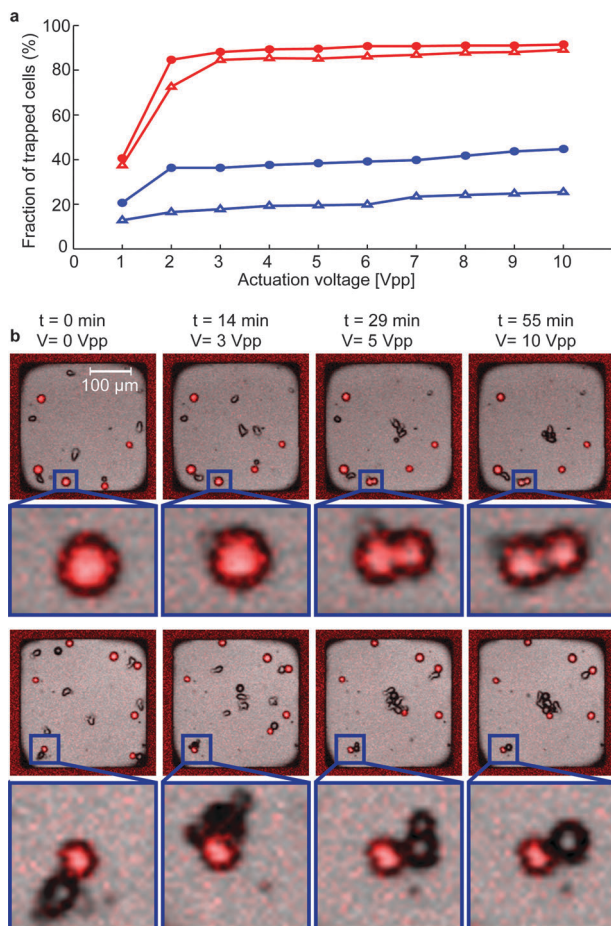


**Fig. 2** Adherent and non-adherent cells show different trapping efficiencies under ultrasonic actuation. (a) Percent trapped adherent (blue lines) and non-adherent (red lines) cells for different actuation voltages. Two sets of experiments were performed with a mixture of adherent 293T cells ( $n = 279$ , triangles and 255, circles) and non-adherent 221 cells ( $n = 412$ , triangles and 433, circles). (b) Time-lapse of two wells containing adherent 293T cells stained with calcein green (shown in red) and non-adherent 221 cells (unstained) at different actuation voltages as indicated. A 293T cell was observed to divide (rows 1 and 2). A 221 cell bound to an adherent 293T cell was seen to reorient towards the trapping position at the center of the well (rows 3 and 4).

cells and non-adherent human B cells (221) were seeded together into the chip, and the 293T cells were allowed to adhere for approximately one hour. The dependence of trapping on actuation voltage for adherent and non-adherent cells was investigated by gradually increasing the ultrasonic actuation voltage from 0 to 10  $V_{pp}$  whilst images were collected (Fig. 2a, Fig. S1, Movie 1, ESI<sup>†</sup>). Already at low voltage ( $< 2 V_{pp}$ ), the majority of non-adherent 221 cells aggregated to a central position, with a plateau of about 90% cells aggregated at voltages  $> 3 V_{pp}$ . In contrast, even at higher voltages the majority of non-adherent cells were not aggregated, showing that the force of adhesion to the glass was stronger than the aggregation force delivered by the ultrasound. Additionally, 221 cells engaged in cell–cell contact, with adherent 293T cells often remaining attached to the 293T cells despite a gradual amplitude increase in the ultrasonic actuation (Fig. 2b). At times,

such cell conjugates were reoriented so that the 221 cells were positioned towards the trapping node in the center of the well, indicating that while the ultrasonic trapping force affected the 221 cells, they were balanced by the cell–cell contact force. Occasionally, the 293T cells detached from the glass so that the whole conjugate moved into the center of the well. Thus, the force generated by the ultrasound was lower or similar to cell adhesion forces to the substrate or to other cells.

### Rapid and synchronized aggregation in multiple wells

To determine whether rapid, simultaneous aggregation of cells in all 100 wells was possible using ultrasonic actuation, non-adherent cells were seeded, left to settle and subsequently exposed to 10  $V_{pp}$  actuation voltage. This resulted in aggregation of the majority of cells in all 100 wells within minutes, effectively establishing a time zero for all cell–cell interactions.

### Accurate, long-term positioning of cell aggregates

Next, the long-term stability of the cell positioning in the microwells with and without ultrasonic exposure was studied. A mixture of human peripheral blood NK and 221 cells (approximately 10–20 cells per well) were seeded in the chip and allowed to settle at the bottom of the well. The ultrasound was turned on and cell aggregates were formed in each well. After completing a  $4 \times 4$  tile scan covering the whole chip ( $\sim 7$  min) the ultrasound was either kept on or switched off. Cell aggregates were tracked for 17 hours, and the distance between the center of the aggregate and the center of the well was calculated for each time point (Fig. 3a and b, Movies 2 and 3, ESI<sup>†</sup>). The positions of aggregates maintained under continuous ultrasound exposure were offset from the center of the well by on average 35–40  $\mu\text{m}$ , and displaced on average 5  $\mu\text{m}$  from that position over the 17 hour long experiment. In contrast, when ultrasound was turned off, the aggregates gradually moved away from the initial trapping position. The timing and direction of this movement varied between aggregates in the different wells, but on average the aggregates were displaced 50  $\mu\text{m}$  from the initial position during the 17-hour movie. Thus, when ultrasound was kept on, the majority of cell-clusters were retained within  $\sim 10 \mu\text{m}$  of the initial central trapping position, allowing acquisition of multiple high-resolution time-lapse movies in parallel.

### MHC class I accumulates at the inhibitory NK cell synapse when cells are brought together by ultrasound

To test whether ultrasound exposure affected immune synapse formation, we used a previously well-characterized cell system consisting of YTS NK cells transfected to express the inhibitory receptor KIR2DL1 (YTS/KIR1), and 221 B cells transfected to express MHC HLA-Cw6 (cognate ligand to KIR2DL1) tagged with GFP (221/Cw6-GFP).<sup>18</sup> The robust positioning of the ultrasound was used to study NK–target cell conjugates by high-resolution 3D confocal microscopy over time (Fig. S2, Movie 4, ESI<sup>†</sup>). Consistent with formation of inhibitory immune synapses, the HLA-Cw6-GFP protein accumulated at the intercellular contacts between these two cell types (Fig. 3c).

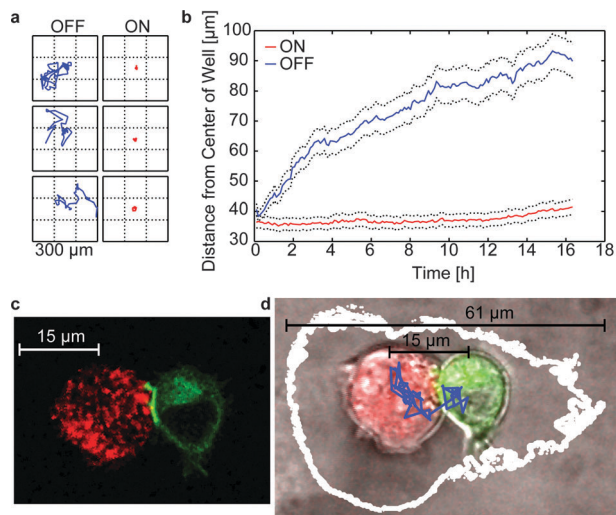


**Fig. 3** NK–target cell clusters are efficiently positioned and maintained close to the center of each well under ultrasound exposure. (a) Spatio-temporal tracking of clusters of human NK cells and 221 target cells in three different wells without (left column) and with (right column) continuous ultrasound exposure (10 V<sub>pp</sub>). In the left column ultrasound was turned off after ~7 minutes. (b) Compiled tracking data of all 100 wells for cell-clusters trapped and released (blue line) or trapped and retained (red line). Dotted black lines represent the standard error of the means. (c) High-resolution confocal fluorescence images of the inhibitory interaction between YTS/KIR1 stained with DDAO (red) and 221/Cw6-GFP showing HLA-Cw6-GFP (green) clustering at the immune synapse. (d) Superposition of 3D reconstructed time lapse images of the inhibitory interaction showing the total area covered by the conjugate during the 2 h-experiment (white borders) and the trajectory of the immune synapse center (blue lines).

The dynamics of HLA-Cw6-GFP at the immune synapse was visualized by 3D rendering of time-lapse sequences and en face projections of the intercellular contact (Fig. S2, ESI<sup>†</sup>). Similar to previous reports,<sup>19</sup> HLA-Cw6-GFP distribution was dynamic, creating different patterns over time, showing that ultrasound exposure did not visibly affect the inhibitory NK cell synapse. The whole NK–target cell conjugate was retained within an area of ~60 × 60 μm<sup>2</sup> over a two hour period, highlighting the robust trapping of the device (Fig. 3d). Furthermore, among 53 immune synapses formed in 33 separate NK–target cell aggregates (≥ 1 synapse/aggregate), we observed no target cell death during continuous ultrasound exposure for at least two hours. These experiments show that the positioning of cells induced by ultrasound-mediated aggregation facilitates high-resolution imaging of cell–cell contacts without affecting important cellular functions such as protein accumulation at the synapse or NK cell inhibition.

### NK cells show heterogeneity in their cytotoxic response towards tumor target cells

The ultrasound device was used to study the capacity of individual NK cells to kill 221 tumor cells. IL-2 activated, human peripheral blood NK cells (Fig. S3, ESI<sup>†</sup>) and 221 cells were seeded in the device and allowed to sediment, prior to scoring the number of cells in each well (Fig. 4a). Cells were seeded to achieve a distribution of approximately one NK cell and 2–4 target cells in each well. In total 402 NK cells and

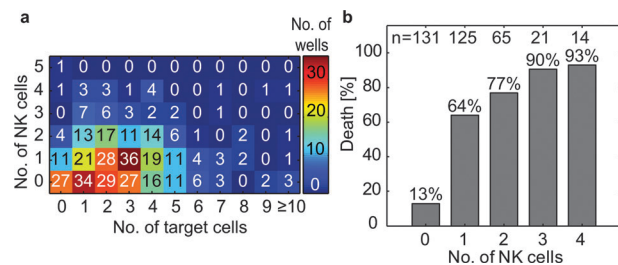


**Fig. 4** Target cell death increases with the number of NK cells per well. (a) Distribution of NK cells and 221 target cells in 400 wells studied. (b) Frequency of wells where target cell death was detected plotted versus the number of NK cells per well. The data are cumulated from four separate experiments using NK cells from two different donors (three experiments with one donor and one experiment with the other donor).

1106 target cells were scored in various effector–target cell combinations. Cell–cell contact was subsequently induced by ultrasound and the interactions in each well were imaged every ~7 minutes for four hours. The chance of target cell death increased with the total number of NK cells present in each well until reaching a plateau: 13% in wells without NK cells, 64% in wells containing 1 NK cell, 77% with 2 NK cells and ~90% with 3 or 4 NK cells (Fig. 4b). The significant increase in target cell death in the presence of NK cells clearly shows that NK cells could kill target cells in the assay. However, not all NK cells were capable of killing target cells, since no killing was observed in 36% of the wells containing single NK cells and at least one target cell. The incremental increase in killing with an increasing number of NK cells shows that the more NK cells present, the more likely it is to have at least one that displays cytotoxic response. Similar to a recently published study<sup>10</sup> these data suggest that NK cells do not cooperate in killing target cells.

Next, we investigated the killing potential of individual NK cells, and thus focused on wells from Fig. 4a that contained single NK cells with 3–10 target cells. Wells with 1–2 targets were excluded from the analysis since the numbers of targets were considered too low to assess the killing capacity of the NK cells. This analysis showed that there was a heterogeneity in individual cells' capacity to kill target cells (Table 1). The killing efficiency of individual NK cells varied significantly, with some cells (18/76) being able to kill three or more target cells in a consecutive fashion during the four-hour long assay, while

**Table 1** Killing capacity of individual NK cells. Light and dark grey areas show the number of events scored for NK cells with low or high cytotoxicity, respectively

Number of target cells \ Number of kills	Number of kills								n	
	0	1	2	3	4	5	6	7		8
3	8	13	7	8	—	—	—	—	—	36
4	6	4	6	3	0	—	—	—	—	19
5	5	2	1	1	0	1	1 <sup>a</sup>	—	—	11
6	0	1	1	1	1	0	0	—	—	4
7	1	1	0	1	0	0	0	0	—	3
8–10	2	0	0	1	0	0	0	0	0	3

<sup>a</sup> One target cell divided.

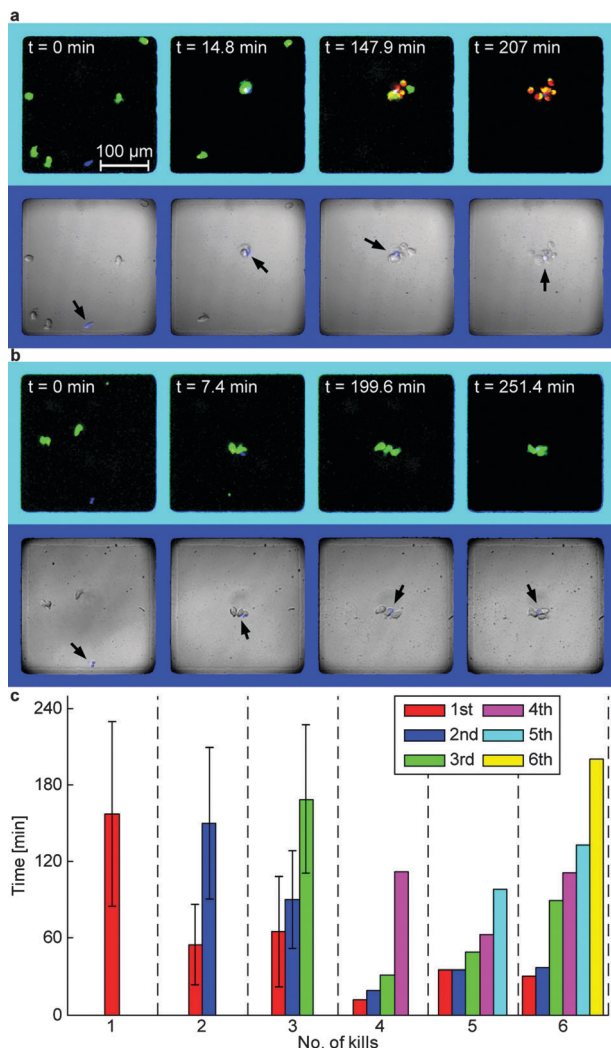


**Fig. 5** Primary human NK cells show great variability in their capacity to kill tumor cells. (a and b) Time-lapse sequences showing fluorescence (top rows) and bright-field (bottom rows) images of a NK serial killer (a) and a non-cytotoxic NK cell (b). Target cell death can be identified by color transition from green to red in the fluorescence image. NK cells are shown in blue and marked with arrows in the bright field images. (c) Timing of the killing events displayed in Table 1. The bars represent time from cluster formation until target cell death was observed (mean and standard deviation for 1–3 kills). The different colors of the bars represent the order of the NK mediated target cell death within a cluster with red representing the first kills, blue the second, green the third, magenta the fourth, cyan the fifth, and yellow the sixth, respectively.

other NK cells were observed not to kill at all (22/76) (see examples of time-lapse movies in Fig. 5a and b and Movies 5 and 6, ESI<sup>†</sup>). This heterogeneity is consistent with other data where NK cells and tumor target cells were confined in micro-wells, and allowed to spontaneously interact while imaged in a time-lapse fashion.<sup>10,14</sup> NK cells and cytotoxic T lymphocytes with extraordinary capacity to kill target cells (termed ‘serial killers’) have been observed before.<sup>3,14,20,21</sup> When quantifying killing over time, we found that NK cells killing up to two target cells showed a frequency of one kill every ~1–3 h, while serial killers (here defined as killing three or more targets during the

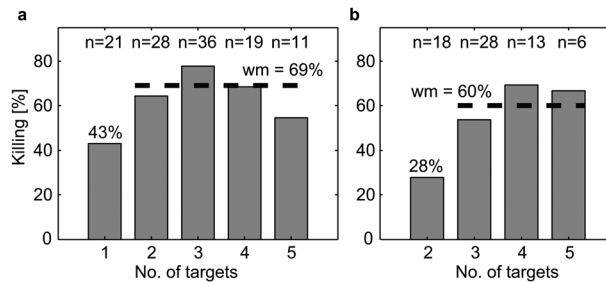


**Fig. 6** The cytotoxic response of individual NK cells depends on the number of simultaneous contacts with target cells. (a) Percentage of wells containing single NK cells and varying number (1–5) of target cells where killing was detected. The NK killing efficiency was observed to increase from 43% in wells containing one target to 69% in wells with two or more targets ( $P < 0.05$ ). (b) Similar analysis was performed in wells where the NK cells had already killed a first target. The killing efficiency of NK cells increased from 28% in wells with one remaining live target cell (two from the beginning as shown on the x-axis) to 60% in wells with two or more live target cells remaining ( $P < 0.05$ ).

assay time of four hours) killed a target every ~0.5–1 h. Thus, activated human primary NK cells show a great heterogeneity in their cytotoxic response with a significant fraction of inactive cells and some serial killers capable of killing several targets within a time frame of a few hours.

### The responsiveness of human primary NK cells increases with stimulatory input from several target cells

Next, we investigated how the responsiveness of individual NK cells depended on the level of stimulatory input from target cells. By assessing the likelihood of killing in wells with single NK cells and varying numbers of targets (*i.e.* wells along the second row from the bottom in Fig. 4a), we observed that the chance of NK cell killing was 43% when one target cell was present, and increased to 64% with two target cells (Fig. 6a). When all cases with more than two target cells were pooled, a plateau was reached with killing occurring in 69% (weighted mean value) of the cases. Statistical analysis showed that the difference observed going from one to several target cells was significant ( $p < 0.05$ ), also when the level of spontaneous cell death (5%) was considered. When analyzing only NK cells that had committed a first kill we made a similar observation, *i.e.* if there was more than one target cell still alive in the well it was more likely that a second kill was observed (Fig. 6b). This difference was also statistically significant showing killing efficiency increasing from 28% to 60%. Thus, NK cytotoxicity was more likely to occur if several live target cells were present in the NK–target cell aggregate.

## Discussion

Here we have utilized a novel ultrasonic method for gentle time-controlled induction of cell–cell contact in one hundred parallel wells for studies of NK–target cell interactions. In conventional imaging approaches *in vitro* where NK and target cells are studied in suspension, it is often difficult to acquire high-resolution data extending over longer times due to cell

migration and fluidic drift. We recently showed that there are significant differences between how NK cells migrate and also transient differences in the individual cells' migration pattern.<sup>13</sup> The migration properties are also an important dynamic factor that can regulate individual cells' capacity to find and kill target cells. However, such data are complex and difficult to interpret. Here we bypassed migration and used ultrasonic standing waves to rapidly and gently bring NK and target cells in contact, achieving a well-determined starting time of the conjugation. By high-resolution time-lapse imaging at several positions, parallel NK–target cell interactions could be studied in detail. This was demonstrated by 4D confocal imaging of the dynamics of protein clustering in the target cell membrane of a NK cell immune synapse.

In previous studies, other groups have measured the forces required to pull apart two conjugated cells to be in the range of ~100 nN.<sup>22</sup> Ultrasonic radiation forces in devices similar to ours have previously been measured to be in the order of 10–1000 pN.<sup>23</sup> These results are calculated from indirect measurements of the energy density by studying the migration of beads or cells in one-dimensional systems.<sup>24–26</sup> In multiwell plates we have recently measured the ultrasonic forces to be up to 50 pN.<sup>15</sup> Based on these studies, we may conclude that ultrasound can be tuned to gently aggregate cells that have not adhered inside the microwells. Thus, the ultrasound forces are significant for generating cell–cell contacts, but not strong enough to interfere with biological forces responsible for, *e.g.*, cell–cell or cell–substrate adhesion.

By screening wells containing IL-2 activated human peripheral blood NK cells and tumor target cells, we could quantify the cytotoxic response of individual NK cells and observed a significant heterogeneity. Despite several days of activation, only a fraction of the NK cells killed target cells in the four-hour long assay. Among the NK cells that did kill we found a sub-population that responded strongly by killing several target cells each. Such 'serial killers' have been described before<sup>3,14</sup> but so far it is unknown if these cells represent a particular subpopulation that could be identified by specific molecular markers. It has recently been shown that CD56<sup>dim</sup> and CD57<sup>+</sup> represent mature, differentiated NK cells<sup>27,28</sup> and it is possible that serial killers are more frequently of that phenotype, but experimental evidence for this is lacking. It is also not known to what extent the frequency of serial killers varies between individuals. This and similar questions could be addressed in the future by using FACS sorted NK cell subpopulations from separate donors in the assay described here.

An interesting observation we make is that individual NK cells were more prone to kill if they were interacting with several susceptible target cells. This could be due to heterogeneity of the target cells, so that with an increasing number of target cells it would be more likely that one or several are sensitive to killing. Alternatively, the NK cell responsiveness could be increased when receiving stimulatory input from several target cells simultaneously. Such a mechanism could be useful *in vivo* since NK cells entering areas with high density of susceptible targets, *e.g.* tumors, would get more responsive.

There is still a lack in understanding between the response of individual NK cells and that of whole cell populations. It is also not well known how transient and dynamic behaviors of NK cells influence experimental readouts. In order to bridge that gap it is important to develop assays as the one presented here, allowing studies of high numbers of cells in parallel, over time and at the single cell level. The described tool is of course not restricted to studies of immune cells but could also be used for several other applications where cell–cell interactions are important.

## Acknowledgements

We thank the Swedish Foundation for Strategic Research, the Swedish Research Council, the Göran Gustafsson Foundation, the Jeansson Foundation, the Clas Groschinsky Foundation and the Åke Wiberg Foundation for financial support.

## References

- 1 P. Höglund and P. Brodin, Current perspectives of natural killer cell education by MHC class I molecules, *Nat. Rev. Immunol.*, 2010, **10**, 724–734.
- 2 H. G. Ljunggren and K. J. Malmberg, Prospects for the use of NK cells in immunotherapy of human cancer, *Nat. Rev. Immunol.*, 2007, **7**, 329–339.
- 3 R. Bhat and C. Watzl, Serial killing of tumor cells by human natural killer cells – enhancement by therapeutic antibodies, *PLoS One*, 2007, **2**, e326.
- 4 P. Brodin, T. Lakshmikanth, S. Johansson, K. Kärre and P. Höglund, The strength of inhibitory input during education quantitatively tunes the functional responsiveness of individual natural killer cells, *Blood*, 2009, **113**, 2434–2441.
- 5 M. Yawata, *et al.*, MHC class I-specific inhibitory receptors and their ligands structure diverse human NK-cell repertoires toward a balance of missing self-response, *Blood*, 2008, **112**, 2369–2380.
- 6 P. J. Lee, P. J. Hung, R. Shaw, L. Jan and L. P. Lee, Microfluidic application-specific integrated device for monitoring direct cell–cell communication via gap junctions between individual cell pairs, *Appl. Phys. Lett.*, 2005, **86**.
- 7 A. M. Skelley, O. Kirak, H. Suh, R. Jaenisch and J. Voldman, Microfluidic control of cell pairing and fusion, *Nat. Methods*, 2009, **6**, 147–152.
- 8 B. Vanherberghen, *et al.*, Ultrasound-controlled cell aggregation in a multi-well chip, *Lab Chip*, 2010, **10**, 2727–2732.
- 9 E. Forslund, *et al.*, Novel Microchip-Based Tools Facilitating Live Cell Imaging and Assessment of Functional Heterogeneity within NK Cell Populations, *Front. Immunol.*, 2012, **3**, 300.
- 10 Y. J. Yamanaka, *et al.*, Single-cell analysis of the dynamics and functional outcomes of interactions between human natural killer cells and target cells, *Integr. Biol.*, 2012, **4**, 1175–1184.
- 11 K. Guldevall, *et al.*, Imaging immune surveillance of individual natural killer cells confined in microwell arrays, *PLoS One*, 2010, **5**, e15453.

- 12 N. Varadarajan, *et al.*, A high-throughput single-cell analysis of human CD8<sup>+</sup> T cell functions reveals discordance for cytokine secretion and cytolysis, *J. Clin. Invest.*, 2011, **121**, 4322–4331.
- 13 M. A. Khorshidi, *et al.*, Analysis of transient migration behavior of natural killer cells imaged *in situ* and *in vitro*, *Integr. Biol.*, 2011, **3**, 770–778.
- 14 B. Vanherberghen, *et al.*, Classification of human natural killer cells based on migration behavior and cytotoxic response, *Blood*, 2013, DOI: 10.1182/blood-2012-06-439851.
- 15 M. Ohlin, A. E. Christakou, T. Frisk, B. Önfelt and M. Wiklund, Influence of acoustic streaming on ultrasonic particle manipulation in a 100-well ring-transducer microplate, *J. Micromech. Microeng.*, 2013, **23**.
- 16 T. W. Frisk, M. A. Khorshidi, K. Guldevall, B. Vanherberghen and B. Onfelt, A silicon-glass microwell platform for high-resolution imaging and high-content screening with single cell resolution, *Biomed. Microdevices*, 2011, **13**, 683–693.
- 17 R. G. Miller and M. Dunkley, Quantitative analysis of the <sup>51</sup>Cr release cytotoxicity assay for cytotoxic lymphocytes, *Cell. Immunol.*, 1974, **14**, 284–302.
- 18 D. M. Davis, *et al.*, The human natural killer cell immune synapse, *Proc. Natl. Acad. Sci. U. S. A.*, 1999, **96**, 15062–15067.
- 19 L. M. Carlin, K. Eleme, F. E. McCann and D. M. Davis, Intercellular transfer and supramolecular organization of human leukocyte antigen C at inhibitory natural killer cell immune synapses, *J. Exp. Med.*, 2001, **194**, 1507–1517.
- 20 S. Isaz, K. Baetz, K. Olsen, E. Podack and G. M. Griffiths, Serial killing by cytotoxic T lymphocytes: T cell receptor triggers degranulation, re-filling of the lytic granules and secretion of lytic proteins *via* a non-granule pathway, *Eur. J. Immunol.*, 1995, **25**, 1071–1079.
- 21 E. Martz, Multiple target cell killing by the cytolytic T lymphocyte and the mechanism of cytotoxicity, *Transplantation*, 1976, **21**, 5–11.
- 22 V. Maruthamuthu, B. Sabass, U. S. Schwarz and M. L. Gardel, Cell–ECM traction force modulates endogenous tension at cell–cell contacts, *Proc. Natl. Acad. Sci. U. S. A.*, 2011, **108**, 4708–4713.
- 23 M. Wiklund, *et al.*, Ultrasonic standing wave manipulation technology integrated into a dielectrophoretic chip, *Lab Chip*, 2006, **6**, 1537–1544.
- 24 R. Barnkob, P. Augustsson, T. Laurell and H. Bruus, Measuring the local pressure amplitude in microchannel acoustophoresis, *Lab Chip*, 2010, **10**, 563–570.
- 25 P. Augustsson, R. Barnkob, S. T. Wereley, H. Bruus and T. Laurell, Automated and temperature-controlled micro-PIV measurements enabling long-term-stable microchannel acoustophoresis characterization, *Lab Chip*, 2011, **11**, 4152–4164.
- 26 R. Barnkob, I. Iranmanesh, M. Wiklund and H. Bruus, Measuring acoustic energy density in microchannel acoustophoresis using a simple and rapid light-intensity method, *Lab Chip*, 2012, **12**, 2337–2344.
- 27 N. K. Bjorkstrom, *et al.*, Expression patterns of NKG2A, KIR, and CD57 define a process of CD56dim NK-cell differentiation uncoupled from NK-cell education, *Blood*, 2010, **116**, 3853–3864.
- 28 S. Lopez-Verges, *et al.*, CD57 defines a functionally distinct population of mature NK cells in the human CD56dimCD16<sup>+</sup> NK-cell subset, *Blood*, 2010, **116**, 3865–3874.